On the Properties of $\alpha/\alpha + \beta$ Diffusion Couples

W. J. Boettinger, S. R. Coriell, C. E. Campbell

Metallurgy Division

and

G. B. McFadden

Mathematical and Computational Science Division

National Institute of Standards and Technology

Gaithersburg, MD 20899, USA

September 28, 1999

Abstract

The properties of diffusion couples in a ternary system are examined theoretically when one end member is composed of single-phase material (α) and the other end member is composed of two-phase material ($\alpha + \beta$). Using the model of Morral and co-workers, we examine the cases in which the two-phase region either grows or dissolves. We prove that when the two-phase material grows, there can be no jump in concentration (or phase fraction of β) at the boundary between the two materials. When it dissolves a jump is necessary. We present numerical examples to demonstrate this result. We also show how the diffusion path varies depending on the composition of the single-phase α end member for a fixed $\alpha + \beta$ end member composition. Under some conditions, three solutions are found for the same initial end member compositions. When these multiple solutions exist, either two or three are virtual (path involves supersaturation). Whenever all three solutions are virtual, a single solution with three interfaces can be found. In this case an intermediate layer of α phase forms within the $\alpha + \beta$ material to relieve the supersaturation.

1 Introduction

A common method to study the interdiffusion of metals is through the use of diffusion couples, where two alloys of different composition are joined at time $t = 0$ at a sharp planar interface located at $x = 0$ and are subjected to a heat treatment at a fixed elevated temperature. Study and analysis of these couples are useful to obtain phase diagram and diffusion data and to gain insight into practical situations such as diffusion bonding, soldering, brazing, oxidation and corrosion. In many cases the two halves are sufficiently long that the analysis can assume that the joined sample extends to infinity in both directions. In this case, similarity solutions involving the variable $x/\sqrt{t}$ may be possible. In binary systems, similarity solutions can describe the interdiffusion in couples composed of the same phase. Similarity solutions can also describe the motion of planar interfaces separating any number of single-phase regions and their (one-dimensional) composition profiles, if the diffusion coefficients are constant and the concentrations of the interfaces are fixed, say by the phase diagram [1]. The same is true for ternary and higher order systems, despite the fact that the interface compositions, while restricted by the isothermal section of the phase diagram, can only be determined from the solution [2]. In ternary systems, it is also well-known that the computed concentrations from such analyses can be virtual; i.e., the composition of a phase can enter an adjacent two-phase region of the phase diagram. Under such circumstances the planar layers may not be morphologically stable [3] and experimentally the interface may proceed through a sequence of microstructures that lead to regions (still defined by the x variable), where the microstructure is two-phase. Multiple solutions can also occur [4]; i.e., more than one solution is found for the same end member concentrations. Often some or all of these multiple solutions are found to be virtual, as we will discuss below.

Expanding an approach presented by Roper and Whittle [5], Morral and coworkers [6,7] have developed a model that treats the situation where end members may be multiphase and/or where new regions forming between the end members may be assumed to be two-phase from time zero. In other words, the morphological stability is not treated and the microstructure is assumed to form the appropriate equilibrium two-phase mixture according to the local average concentration in the two-phase field of the phase diagram. Here the local average concentration is defined on an appropriately coarse scale and the small concentration differences due to the Gibbs-Thomson effect (and hence Ostwald ripening) are neglected. In this case the motion of the "interfaces" separating single and multiphase "layers" can also be analyzed with similarity solutions. Morral et al. [8] have classified the various types of boundaries possible according to the change in the number of phases that occurs when an interface is crossed in the microstructure. In this paper, we examine in detail the predictions of this model for diffusion couples initially composed of two halves: a single-phase α material of uniform concentration and an $\alpha + \beta$ material of constant average concentration (phase fraction).

In binary systems, similarity solutions for diffusion couples of the $\alpha/\alpha + \beta$ type have been detailed by Sekerka [1]. Since the chemical potentials are fixed in a two-phase region in a binary at fixed temperature (and pressure), there can be no diffusion in the two phase region (neglecting Ostwald ripening effects). As long as the adjacent single-phase region is not supersaturated (as from a quench from higher temperature), the concentration gradient that develops during the diffusion process in the single-phase region will always cause the two-phase region to dissolve. Thus, a jump will occur across the boundary between the composition of the single-phase material and the average composition of the two-phase material. The existence of this jump also implies a jump in phase fraction of the β phase from zero in the α phase to a nonzero value in the $\alpha + \beta$ mixture.

In ternary systems, chemical potential gradients are possible in a two-phase region, diffusion can occur and the interface can migrate in either direction. It has been noted by several authors [5, 6, 9] that when the $\alpha + \beta$ material dissolves, a jump in the concentrations must be present, just like the binary case. Indeed couples of $\alpha/\alpha + \beta$ type, have been studied by Beriot [6] who obtained excellent agreement between the model and experimental results for cases where the $\alpha + \beta$ mixture is dissolving. No results are presented for the growing case. However, it has been observed in numerical solutions using the code DICTRA [10] that when the two-phase mixture grows there is no jump in concentration (or phase fraction of β). In this paper we prove this numerical observation.

In addition, Morral and coworkers have described microstructure maps for diffusion couples [11]. With one end member composition fixed, a map specifies the range of the other end member composition where diffusion couples will have the same microstructure. Identical microstructures have layers composed of the same phase sequence and the same direction of interface motion. The boundaries separating compositions with identical behavior are superimposed on the phase diagram. Maps of this type have been determined experimentally for $\alpha/\alpha+\beta$ couples [12]. In this paper we compute such a map and examine the nature of the transitions of the diffusion solutions near the map boundaries.

2 Theory

We use the model described by Hopfe and Morral [7] to treat $\alpha+\beta/\alpha+\beta$ diffusion paths, but apply it to $\alpha/\alpha+\beta$ paths, with a modified notation for added clarity in this context. We assume the α phase is initially in the region $x<0$, and the $\alpha+\beta$ two-phase material is initially in the region $x>0$. The model treats diffusion in the single-phase α region in the usual way, where the fluxes J_1^α and J_2^α of the species 1 and 2 are given in terms of the gradients of the concentrations C_1^α and C_2^α by

$$J_1^\alpha = -D_{11}\frac{\partial C_1^\alpha}{\partial x} - D_{12}\frac{\partial C_2^\alpha}{\partial x} \tag{1}$$

$$J_2^\alpha = -D_{21}\frac{\partial C_1^\alpha}{\partial x} - D_{22}\frac{\partial C_2^\alpha}{\partial x}. \tag{2}$$

For constant diffusion coefficients D_{ij} in the α phase, conservation of solute then requires

$$\frac{\partial C_1^\alpha}{\partial t} = D_{11}\frac{\partial^2 C_1^\alpha}{\partial x^2} + D_{12}\frac{\partial^2 C_2^\alpha}{\partial x^2}, \tag{3}$$

$$\frac{\partial C_2^\alpha}{\partial t} = D_{21}\frac{\partial^2 C_1^\alpha}{\partial x^2} + D_{22}\frac{\partial^2 C_2^\alpha}{\partial x^2}. \tag{4}$$

Diffusion in the two-phase material is modeled by assuming that one can define average concentrations $\bar{C}_1$ and $\bar{C}_2$ of the two-phase mixture at each point. The two-phase mixture is assumed to be locally equilibrated, so that $\bar{C}_1$ consists of a phase-fraction-weighted sum of the concentrations of C_1 in the α and β phases that lie on opposite ends of a tie line, with a similar definition for $\bar{C}_2$. The model further assumes that the fluxes $\bar{J}_1$ and $\bar{J}_2$ of component

1 and 2 are given by the gradients of the α phase concentrations in the two-phase mixture; diffusion in the β phase is ignored. This is clearly most valid when the fraction of β is small. Thus we have in the $\alpha + \beta$ material,

$$\bar{J}_1 = -D_{11}\frac{\partial C_1^\alpha}{\partial x} - D_{12}\frac{\partial C_2^\alpha}{\partial x} \tag{5}$$

$$\bar{J}_2 = -D_{21}\frac{\partial C_1^\alpha}{\partial x} - D_{22}\frac{\partial C_2^\alpha}{\partial x}. \tag{6}$$

The assumption that the two-phase mixture is locally equilibrated implies that knowledge of the average concentrations determines the values of the α-phase concentrations (as well as the β-phase concentrations). Thus, relationships f and g exist such that

$$C_1^\alpha = f(\bar{C}_1, \bar{C}_2) \tag{7}$$

$$C_2^\alpha = g(\bar{C}_1, \bar{C}_2). \tag{8}$$

Using the chain rule, the flux equations can be written in terms of gradients of $\bar{C}_1$ and $\bar{C}_2$ as

$$\bar{J}_1 = -\left[D_{11}\frac{\partial C_1^\alpha}{\partial \bar{C}_1} + D_{12}\frac{\partial C_2^\alpha}{\partial \bar{C}_1}\right]\frac{\partial \bar{C}_1}{\partial x} - \left[D_{11}\frac{\partial C_1^\alpha}{\partial \bar{C}_2} + D_{12}\frac{\partial C_2^\alpha}{\partial \bar{C}_2}\right]\frac{\partial \bar{C}_2}{\partial x} \tag{9}$$

$$\bar{J}_2 = -\left[D_{21}\frac{\partial C_1^\alpha}{\partial \bar{C}_1} + D_{22}\frac{\partial C_2^\alpha}{\partial \bar{C}_1}\right]\frac{\partial \bar{C}_1}{\partial x} - \left[D_{21}\frac{\partial C_1^\alpha}{\partial \bar{C}_2} + D_{22}\frac{\partial C_2^\alpha}{\partial \bar{C}_2}\right]\frac{\partial \bar{C}_2}{\partial x}. \tag{10}$$

If the quantities $(\partial C_i^\alpha/\partial \bar{C}_j)$ and D_{ij} can be treated as constants, conservation of solute gives

$$\frac{\partial \bar{C}_1}{\partial t} = \left[D_{11}\frac{\partial C_1^\alpha}{\partial \bar{C}_1} + D_{12}\frac{\partial C_2^\alpha}{\partial \bar{C}_1}\right]\frac{\partial^2 \bar{C}_1}{\partial x^2} + \left[D_{11}\frac{\partial C_1^\alpha}{\partial \bar{C}_2} + D_{12}\frac{\partial C_2^\alpha}{\partial \bar{C}_2}\right]\frac{\partial^2 \bar{C}_2}{\partial x^2} \tag{11}$$

$$\frac{\partial \bar{C}_2}{\partial t} = \left[D_{21}\frac{\partial C_1^\alpha}{\partial \bar{C}_1} + D_{22}\frac{\partial C_2^\alpha}{\partial \bar{C}_1}\right]\frac{\partial^2 \bar{C}_1}{\partial x^2} + \left[D_{21}\frac{\partial C_1^\alpha}{\partial \bar{C}_2} + D_{22}\frac{\partial C_2^\alpha}{\partial \bar{C}_2}\right]\frac{\partial^2 \bar{C}_2}{\partial x^2}. \tag{12}$$

Eqn. (11) and Eqn. (12) must be solved in the $\alpha + \beta$ material and Eqn. (3) and Eqn. (4) must be solved in the α phase material subject to initial conditions representing the two end member compositions and conditions at the interface.

Under the assumption of equilibrium at the $\alpha/\alpha + \beta$ interface, the interface values of

(C_1^α,C_2^α) and $(\bar{C}_1,\bar{C}_2)$, namely, $(C_{1I}^\alpha,C_{2I}^\alpha)$ and $(\bar{C}_{1I},\bar{C}_{2I})$, must lie at the end of and at a point on the same tie line in the two-phase region, respectively, as also given by Eqn. (7) and Eqn. (8). In addition, conservation of solute requires that the jumps in concentration at the $\alpha/\alpha+\beta$ interface be related to the velocity of the interface, V, by

$$V(\bar{C}_{1I} - C_{1I}^\alpha) = \bar{J}_1 - J_1^\alpha \tag{13}$$

$$V(\bar{C}_{2I} - C_{2I}^\alpha) = \bar{J}_2 - J_2^\alpha, \tag{14}$$

where positive V is dissolution of the $\alpha+\beta$ material.

We consider an isothermal section of a phase diagram where the $\alpha+\beta$ region is bounded by parallel straight lines. The α phase region is defined by

$$sC_1^\alpha + C_2^\alpha < A, \tag{15}$$

and the $\alpha+\beta$ phase region is defined by

$$s\bar{C}_1 + \bar{C}_2 > A \tag{16}$$

and

$$s\bar{C}_1 + \bar{C}_2 < B, \tag{17}$$

where s, A, and B are positive constants with $A < B$. The tie-lines restricting the values of $(\bar{C}_1,\bar{C}_2)$ and (C_1^α,C_2^α) in the two-phase mixture are taken to be

$$(\bar{C}_2 - C_2^\alpha) = r(\bar{C}_1 - C_1^\alpha), \tag{18}$$

where $r \neq -s$ is a constant and the expression, $sC_1^\alpha + C_2^\alpha = A$, restricts the values of (C_1^α,C_2^α) possible in two-phase mixtures. For this special case, the tie lines are assumed to be parallel. The functions f and g, Eqn. (7) and Eqn. (8) become

$$C_1^\alpha = \frac{A + r\bar{C}_1 - \bar{C}_2}{r+s} \tag{19}$$

and

$$C_2^{\alpha} = \frac{rA - rs\bar{C}_1 + s\bar{C}_2}{r+s}. \tag{20}$$

The flux equations, Eqn. (9) and Eqn. (10), in the two-phase material become

$$\bar{J}_1 = -\left[\frac{rD_{11} - rsD_{12}}{r+s}\right]\frac{\partial \bar{C}_1}{\partial x} - \left[\frac{-D_{11} + sD_{12}}{r+s}\right]\frac{\partial \bar{C}_2}{\partial x} \tag{21}$$

and

$$\bar{J}_2 = -\left[\frac{rD_{21} - rsD_{22}}{r+s}\right]\frac{\partial \bar{C}_1}{\partial x} - \left[\frac{-D_{21} + sD_{22}}{r+s}\right]\frac{\partial \bar{C}_2}{\partial x} \tag{22}$$

while the diffusion equations in the two-phase material become

$$\frac{\partial \bar{C}_1}{\partial t} = \left[\frac{rD_{11} - rsD_{12}}{r+s}\right]\frac{\partial^2 \bar{C}_1}{\partial x^2} + \left[\frac{-D_{11} + sD_{12}}{r+s}\right]\frac{\partial^2 \bar{C}_2}{\partial x^2} \tag{23}$$

$$\frac{\partial \bar{C}_2}{\partial t} = \left[\frac{rD_{21} - rsD_{22}}{r+s}\right]\frac{\partial^2 \bar{C}_1}{\partial x^2} + \left[\frac{-D_{21} + sD_{22}}{r+s}\right]\frac{\partial^2 \bar{C}_2}{\partial x^2} \tag{24}$$

We note that the matrix of the effective diffusion coefficients in the two-phase region has eigenvalues of $\{0, (rD_{11} - rsD_{12} - D_{21} + sD_{22})/(r+s)\}$ and eigenvectors $\{[1/r, 1], [(D_{11} - sD_{12})/(D_{21} - sD_{22}), 1]\}$, which lie along the tie line and at an angle to it, respectively. The zero eigenvalue arises because no diffusion is possible in the direction of the tie line since the chemical potentials do not change along the tie line. We note that the second eigenvector does not depend on r, the slope of the tie-lines. The expressions (19) and (20), with subscript "I" added, are also used to restrict the interface concentrations. Chen and Morral [13] give a generalization of this diffusion matrix when the tie lines are not parallel.

3 Composition Jumps at the $\alpha/\alpha + \beta$ Interface

To gain information on the possible jump conditions at the $\alpha/\alpha+\beta$ interface, we manipulate the two flux continuity equations, Eqn. (13) and Eqn. (14). After multiplying by appropriate factors and adding, one can eliminate the quantities $(\partial\bar{C}_1/\partial x)$ and $(\partial\bar{C}_2/\partial x)$ and obtain the single equation

$$V\left[s\bar{C}_{1I}+\bar{C}_{2I}-A\right]\left[\frac{rD_{11}-rsD_{12}-D_{21}+sD_{22}}{r+s}\right]=\left[s\frac{\partial C_1^\alpha}{\partial x}+\frac{\partial C_2^\alpha}{\partial x}\right][D_{11}D_{22}-D_{12}D_{21}] \tag{25}$$

where the gradients are evaluated in the α phase at the $\alpha/\alpha+\beta$ interface.

We now examine the signs of the various terms in this equation:

$$[s\bar{C}_{1I}+\bar{C}_{2I}-A]\geq 0, \tag{26}$$

$$\frac{rD_{11}-rsD_{12}-D_{21}+sD_{22}}{r+s}>0, \tag{27}$$

$$s\frac{\partial C_1^\alpha}{\partial x}+\frac{\partial C_2^\alpha}{\partial x}\geq 0, \tag{28}$$

and

$$D_{11}D_{22}-D_{12}D_{21}>0. \tag{29}$$

The first expression is proportional to the jump in concentration across the interface between the $\alpha+\beta$ material and the α phase, measured along the tie line direction. This is so because $sC_{1I}^\alpha+C_{2I}^\alpha=A$ and $(\bar{C}_{2I}-C_{2I}^\alpha)=r(\bar{C}_{1I}-C_{1I}^\alpha)$. The expression must be positive or zero because the concentration of the two-phase mixture at the interface must lie in the two-phase region of the phase diagram. The second expression is positive definite as shown in the Appendix. It is the nonzero eigenvalue of the diffusion matrix in the $\alpha+\beta$ mixture. The third expression must be non-negative to guarantee that the path in the α phase does not cross into the $\alpha+\beta$ region of the phase diagram at the interface; i.e., to prevent the path from becoming virtual near the interface. The fourth expression is the determinant of the diffusion matrix in the α region and must be positive, since only thermodynamically stable phases are considered (i.e., no spinodal).

When $V<0$, i.e., when the two-phase mixture is growing in size, the only way Eqn. (25) can be satisfied is therefore for both

$$[s\bar{C}_{1I}+\bar{C}_{2I}-A]=0 \tag{30}$$

and

$$s\frac{\partial C_1^\alpha}{\partial x} + \frac{\partial C_2^\alpha}{\partial x} = 0, \tag{31}$$

since otherwise the left hand side of Eqn. (25) is negative and the right hand side is positive. Eqn. (30) requires that $(\bar{C}_{1I}, \bar{C}_{2I})$ lies on the $\alpha/\alpha+\beta$ phase diagram boundary. Thus there can be no jump in concentration between the α phase and the $\alpha+\beta$ mixture at their moving interface and consequently the phase fraction of β must be zero at the moving interface. Furthermore, Eqn. (31) implies that the diffusion path in the α phase when plotted on the isothermal section of the ternary phase diagram is tangent to the $\alpha/\alpha+\beta$ boundary of the phase diagram. Thus the path when the two phase mixture grows, must lie on the verge of becoming virtual; i.e., at the limit to prevent constitutional supersaturation.

When $V > 0$, $s\bar{C}_{1I}+\bar{C}_{2I}-A$ can be any non-negative number and a jump in concentration generally exists. The phase fraction of β at the interface will be nonzero and the diffusion path in the α region will not be tangent to the phase boundary.

4 Numerical Calculations

We carry out numerical solutions for the interface velocity and diffusion fields for a specific case. For simplicity we neglect off-diagonal diffusion terms in the α phase for the remainder of this paper so that $D_{12} = D_{21} = 0$. Further, we assume that the parameters s and r are unity so that the phase boundary and tie lines are orthogonal. With these restrictions, the matrix of diffusion coefficients in the two-phase region has eigenvalues of $\{0, (D_{11} + D_{22})/2\}$ and eigenvectors $\{[1, 1], [-D_{11}/D_{22}), 1]\}$. The initial conditions are

$$C_1^\alpha(x, 0) = C_{1\infty}^\alpha, \tag{32}$$

$$C_2^\alpha(x, 0) = C_{2\infty}^\alpha, \tag{33}$$

$$\bar{C}_1(x, 0) = \bar{C}_{1\infty}, \tag{34}$$

and

$$\bar{C}_2(x, 0) = \bar{C}_{2\infty}. \tag{35}$$

The boundary conditions are

$$C_1^\alpha(x \to -\infty, t) = C_{1\infty}^\alpha, \tag{36}$$

$$C_2^\alpha(x \to -\infty, t) = C_{2\infty}^\alpha, \tag{37}$$

$$\bar{C}_1(x \to \infty, t) = \bar{C}_{1\infty}, \tag{38}$$

and

$$\bar{C}_2(x \to \infty, t) = \bar{C}_{2\infty}. \tag{39}$$

We seek solution of this problem where the interface position is given by $X(t) = \lambda\sqrt{t}$. Using Eqn. (1), Eqn. (2), Eqn. (21) and Eqn. (22) for the fluxes, the flux boundary conditions Eqn. (13) and Eqn. (14) for $r = s = 1$ are then

$$(\bar{C}_{1I} - C_{1I}^\alpha)\frac{dX}{dt} = -\tfrac{1}{2}D_{11}\frac{\partial \bar{C}_1}{\partial x} + \tfrac{1}{2}D_{11}\frac{\partial \bar{C}_2}{\partial x} + D_{11}\frac{\partial C_1^\alpha}{\partial x} \tag{40}$$

and

$$(\bar{C}_{2I} - C_{2I}^\alpha)\frac{dX}{dt} = \tfrac{1}{2}D_{22}\frac{\partial \bar{C}_1}{\partial x} - \tfrac{1}{2}D_{22}\frac{\partial \bar{C}_2}{\partial x} + D_{22}\frac{\partial C_2^\alpha}{\partial x}. \tag{41}$$

The solutions for the composition fields in the $\alpha-$phase material, $x < \lambda\sqrt{t}$, with given interface values $C_1^\alpha(\lambda\sqrt{t}, t) = C_{1I}^\alpha$ and $C_2^\alpha(\lambda\sqrt{t}, t) = C_{2I}^\alpha$ are

$$C_1^\alpha = C_{1\infty}^\alpha + (C_{1I}^\alpha - C_{1\infty}^\alpha)\frac{\mathrm{erfc}(-\xi/\sqrt{4D_{11}})}{\mathrm{erfc}(-\lambda/\sqrt{4D_{11}})}, \tag{42}$$

and

$$C_2^\alpha = C_{2\infty}^\alpha + (C_{2I}^\alpha - C_{2\infty}^\alpha)\frac{\mathrm{erfc}(-\xi/\sqrt{4D_{22}})}{\mathrm{erfc}(-\lambda/\sqrt{4D_{22}})}, \tag{43}$$

where $\xi = x/\sqrt{t}$.

In order to determine the solution in the two-phase material where $x > \lambda\sqrt{t}$, it is convenient to define new concentration variables in the directions of the eigenvectors

$$\bar{V}_1 = -\frac{D_{22}(\bar{C}_1 - \bar{C}_2)}{D_{11} + D_{22}} \tag{44}$$

and

$$\bar{V}_2 = \frac{D_{22}\bar{C}_1 + D_{11}\bar{C}_2}{D_{11} + D_{22}}, \tag{45}$$

which can be inverted to give

$$\bar{C}_1 = -\frac{D_{11}\bar{V}_1}{D_{22}} + \bar{V}_2 \tag{46}$$

$$\bar{C}_2 = \bar{V}_1 + \bar{V}_2 \tag{47}$$

Then Eqn. (23) and Eqn. (24) become

$$\frac{\partial \bar{V}_1}{\partial t} = \bar{D}\frac{\partial^2 \bar{V}_1}{\partial x^2} \tag{48}$$

and

$$\frac{\partial \bar{V}_2}{\partial t} = 0, \tag{49}$$

where

$$\bar{D} = \tfrac{1}{2}(D_{11} + D_{22}), \tag{50}$$

the nonzero eigenvalue. The solution with $\bar{V}_1(x,0) = \bar{V}_{1\infty}$ and $\bar{V}_1(\lambda\sqrt{t},t) = \bar{V}_{1I}$ is given by

$$\bar{V}_1 = \bar{V}_{1\infty} + (\bar{V}_{1I} - \bar{V}_{1\infty})\frac{\operatorname{erfc}(\xi/\sqrt{4\bar{D}})}{\operatorname{erfc}(\lambda/\sqrt{4\bar{D}})}. \tag{51}$$

The diffusion coefficient is zero for the second equation (49), due to the zero value of the second eigenvalue. Thus the appropriate boundary conditions to be imposed on $\bar{V}_2$ require special consideration. For $\lambda > 0$ the single condition $\bar{V}_2(x,0) = \bar{V}_{2\infty}$ is imposed, so that the solution is simply $\bar{V}_2(x,t) = \bar{V}_{2\infty}$. For $\lambda < 0$, we impose the conditions $\bar{V}_2(x,0) = \bar{V}_{2\infty}$ and $\bar{V}_2(\lambda\sqrt{t},t) = \bar{V}_{2I}$, which admits the discontinuous solution $\bar{V}_2(x,t) = \bar{V}_{2\infty}$ for $x > 0$ and $\bar{V}_2(x,t) = \bar{V}_{2I}$ for $x < 0$. For either sign of λ, the resulting solution thus can be written in the similarity form

$$\bar{V}_2 = \bar{V}_{2I} + (\bar{V}_{2\infty} - \bar{V}_{2I})S(\xi), \tag{52}$$

where $S(\xi)$ is the Heaviside step function, i.e., $S(\xi) = 0$ for $\xi < 0$ and $S(\xi) = 1$ for $\xi > 0$. As noted by Hopfe and Morral [7], the limiting behavior of the error function as the diffusion coefficient approaches zero is a step function at $\xi = 0$. The flux conditions (40) and (41) can now be written as

$$\lambda(\bar{C}_{1I} + \bar{C}_{2I} - A) =$$

$$D_{11}\left[(\bar{C}_{1I} - \bar{C}_{2I} - \bar{C}_{1\infty} + \bar{C}_{2\infty})\frac{U(\lambda/\sqrt{4\bar{D}})}{\sqrt{\bar{D}}} + (A + \bar{C}_{1I} - \bar{C}_{2I} - 2C^{\alpha}_{1\infty})\frac{U(\lambda/\sqrt{4D_{11}})}{\sqrt{D_{11}}}\right] \quad (53)$$

and

$$\lambda(\bar{C}_{1I} + \bar{C}_{2I} - A) =$$

$$D_{22}\left[-(\bar{C}_{1I} - \bar{C}_{2I} - \bar{C}_{1\infty} + \bar{C}_{2\infty})\frac{U(\lambda/\sqrt{4\bar{D}})}{\sqrt{\bar{D}}} + (A + \bar{C}_{1I} - \bar{C}_{2I} - 2C^{\alpha}_{2\infty})\frac{U(\lambda/\sqrt{4D_{22}})}{\sqrt{D_{22}}}\right], \quad (54)$$

where

$$U(z) = \frac{2}{\sqrt{\pi}\exp(z^2)\mathrm{erfc}(z)}. \quad (55)$$

We have used Eqn. (19) and Eqn. (20) to eliminate the $\alpha-$phase interfacial compositions. We note that the left-hand sides of Eqn. (53) and Eqn. (54) are identical. These two equations contain the three unknowns $\bar{C}_{1I}$, $\bar{C}_{2I}$, and λ. For $\lambda > 0$, we have the additional requirement from Eqn. (52) that $\bar{V}_2 = \bar{V}_{2\infty}$, and thus we have three equations and three unknowns. For $\lambda < 0$, we use the condition $\bar{C}_{1I} + \bar{C}_{2I} = A$ which prevents the $\alpha-$phase diffusion path from entering the $\alpha + \beta$ region at the interface, see Eqn. (25) and the discussion thereafter.

Numerical calculations were performed for $D_{11} = 10D_{22}$, $A = 0.12$, $\bar{C}_{1\infty} = \bar{C}_{2\infty} = 0.07$. Fig. 1 shows the calculated diffusion path for two cases with different values for $(C^{\alpha}_{1\infty}, C^{\alpha}_{2\infty})$: (0.055, 0.055) where the $\alpha + \beta$ mixture dissolves ($\lambda > 0$) and (0.035, 0.08) where the $\alpha + \beta$ mixture grows ($\lambda < 0$). The former exhibits a jump in interface concentrations as indicated by the dashed line. The latter has no jump in interface concentrations at the $\alpha+\beta$ interface. The path in the α region is also tangent to the $\alpha/\alpha + \beta$ phase boundary. Both of these features are consistent with the proof above. The dashed line in this latter case represents a stationary $\alpha + \beta/\alpha + \beta$ interface at $\xi = 0$ as described in [7]; viz., a zig-zag path. Such zig-zag paths can occur due to the step function described in Eqn. (52). It is evident that diffusion paths in the two phase region must be made of jumps along tie lines and straight line segments in the direction of the eigenvector with non-zero eigenvalue.

For any particular set of $(\bar{C}_{1\infty}, \bar{C}_{2\infty})$, the border in the α region that separates values of

($C^\alpha_{1\infty}$,$C^\alpha_{2\infty}$) that exhibit growth as opposed to dissolution can be obtained by letting $\lambda = 0$ in the above equations. After some manipulation, the border is found to be a straight line given by

$$C^\alpha_{2\infty} - \frac{1}{2}(A + \bar{C}_{1\infty} - \bar{C}_{2\infty}) = -\left[\frac{\sqrt{D_{22}} + \sqrt{(D_{11} + D_{22})/2}}{\sqrt{D_{11}} + \sqrt{(D_{11} + D_{22})/2}}\right]\left[C^\alpha_{1\infty} - \frac{1}{2}(A - \bar{C}_{1\infty} + \bar{C}_{2\infty})\right]. \tag{56}$$

The line passes through the point $([A - \bar{C}_{1\infty} + \bar{C}_{2\infty}]/2, [A + \bar{C}_{1\infty} - \bar{C}_{2\infty}]/2)$, which is the point (0.06, 0.06) in the case shown in Fig. 1. This point lies on the $\alpha/\alpha+\beta$ boundary that is the end of the tie line through $(\bar{C}_{1\infty}, \bar{C}_{2\infty})$. We note that if $D_{11} = D_{22}$, the $\lambda = 0$ line is identical to the $\alpha/\alpha + \beta$ boundary of the phase diagram. In this case the $\alpha + \beta$ material will dissolve for any composition of α phase. This behavior is identical to a binary alloy. Roughly speaking, the two-phase mixture will grow in a ternary alloy, when a significant component of the vector connecting the end member compositions lies in the direction of the eigenvector corresponding to the non-zero eigenvalue.

The plots of concentration vs. ξ corresponding to Case 1 and 2 (Fig. 1) are shown in Figs. 2 and 3. The values of ξ and λ in these and later figures are shown normalized with respect to $\sqrt{D_{22}}$. The large ratio of D_{11}/D_{22} leads to the increased penetration of component 1. Figs. 4 and 5 show plots of phase fraction of β along with schematic diffusion microstructures. A discontinuity in phase fraction exists when the $\alpha + \beta$ mixture dissolves (Fig. 4). There is no discontinuity in phase fraction at the moving interface when the $\alpha + \beta$ mixture grows, but a discontinuity exists at the $\xi = 0$ stationary interface (Fig. 5).

In the notation of Morral and co-workers, these two cases are described by the expressions $\alpha > \alpha + \beta$ and $\alpha < \alpha + \beta|\alpha + \beta$, ($\lambda > 0$ and $\lambda < 0$, respectively). The direction of the inequality symbol indicates the direction of motion of the interface with respect to the two adjacent layers. The vertical bar represents a stationary interface at $\xi = 0$. In this paper with the $\alpha + \beta$ mixture initially in the region $x > 0$, the "greater than symbol" indicates $\lambda > 0$, motion of the interface in the positive x-direction and dissolution of the mixture. This notation will be used in the remainder of this paper.

5 Multiple Solutions

For some α phase end member compositions near the $\lambda = 0$ line, there exist multiple solutions for λ. Values of λ were calculated for $\overline{C}_{1\infty} = \overline{C}_{2\infty} = 0.07$ and $C^{\alpha}_{2\infty} = 0.082$ when $C^{\alpha}_{1\infty}$ is varied between 0.02 and 0.038, the later concentration lying on the two-phase boundary. These results are shown in Fig. 6. Multiple solutions exist for $0.0238 < C^{\alpha}_{1\infty} < 0.0255$ as indicated by the "S"-shaped part of the curve (between points a and e in Fig. 6). The beginning of this range corresponds to the value of $C^{\alpha}_{1\infty}$ where there also exists a $\lambda = 0$ solution. Thus the range of α phase end member concentrations where multiple solutions exist, when plotted on the phase diagram, lie at values of $C^{\alpha}_{1\infty}$ greater than those given by the $\lambda = 0$ line shown in Fig. 1. Note that when there are three solutions, two have positive values of λ (dissolution of $\alpha + \beta$) and one has a negative value (growth of $\alpha + \beta$). As the value chosen for $C^{\alpha}_{2\infty}$ is increased, the "S"-shaped feature disappears in plots of λ vs. $C^{\alpha}_{1\infty}$, and there exists only one solution.

The multiple solution results are summarized on the phase diagram in Fig. 7. Straight lines are displayed that give the α phase end member compositions, $(C^{\alpha}_{1\infty}, C^{\alpha}_{2\infty})$ for specified values of λ for $\overline{C}_{1\infty} = \overline{C}_{2\infty} = 0.07$. The lines for negative λ radiate out from (0.06, 0.06) and never intersect. The lines for positive values of λ, as increasing from zero, move to the left of a point, denoted P, with increasing steepness. In a region of concentrations to the left of point P, three solutions exist as seen from the possibility of three intersecting constant λ lines, two with positive λ and one with negative λ. The point P has a special value for $C^{\alpha}_{1\infty}$ given by

$$C^{\alpha}_{1\infty} = \frac{2AD_{11} + (A - \overline{C}_{1\infty} - \overline{C}_{2\infty})\sqrt{2D_{11}(D_{11} + D_{22})} - 2(D_{11}\overline{C}_{2\infty} + D_{22}\overline{C}_{1\infty})}{2(D_{11} - D_{22})}. \quad (57)$$

This value was determined by expanding the general expression (not given) for lines of constant λ about $\lambda = 0$. The value of $C^{\alpha}_{2\infty}$ at point P can be found from Eqn. (56). For the present case this gives (0.0313, 0.0775).

6 Virtual Solutions

For the part of the dashed curve between the two bold points (b and f) in Fig. 6 , the associated diffusion paths are virtual. This was determined for each λ value by numerical examination of the location of the diffusion path compared to the phase diagram. Note that in part of the multiple solution range between the points a and b (i.e., $0.0238 < C^{\alpha}_{1\infty} < 0.0246$), the diffusion path for the solution with the largest λ value is not virtual. Elsewhere in the multiple solution range, the diffusion paths are all found to be virtual in one way or another. Specifically, for λ values between points b and c, the α-phase concentrations enter into the two-phase region of the phase diagram. The path for negative λ values between points d and f is virtual by the entry of the two-phase concentration into the α region. The diffusion path for values of λ between points c and d exhibits both types of virtuality. Note that between points e and f only one solution exists, but it is virtual.

Fig. 8 summarizes the regions of the phase diagram where multiple and virtual solutions exist. The boundary PT is part of the $\lambda = 0$ line. The boundaries PQ and PS were determined by numerical examination of the virtuality of the diffusion paths. The boundary PR was determined from the envelope of constant λ lines shown in Fig. 7. In the singly-hatched lower region SPT, there are three solutions; two are virtual and one is non-virtual. The non-virtual solution has a positive value of λ; i.e., the two phase material dissolves. In the double-cross-hatched region RPS there are three solutions, and all are virtual. In the singly-hatched upper region RPQ there is only one solution but it is virtual.

It is useful to examine the two diffusion paths when the α phase end member composition is located at the special points P and Q (Fig. 9). The nature of these paths is most easily described by considering how the Case 2 path of Fig. 1 would vary as the α phase end member composition is moved to these points. For point P, the zig-zag portion of the path in the $\alpha + \beta$ material disappears and the path in the α phase remains the tangent to the $\alpha/\alpha + \beta$ boundary of the phase diagram (no jump at the interface). Further end member composition change into region SPT or RPS causes the development of multiple and/or virtual paths as described above. For point Q, the portion of the path in the α phase disappears and the path is a zig-zag lying wholly in the $\alpha + \beta$ material. Further end member composition change into region RPQ causes the zig-zag path to become virtual by penetration into the α phase region of the phase diagram. The coordinates of point Q are obtained from a simple geometric analysis as

$$C_1 = \frac{(\bar{C}_{1\infty} + 3\bar{C}_{2\infty} - 3A) + [D_{22}/D_{11}](3\bar{C}_{1\infty} + \bar{C}_{2\infty} - A)}{2([D_{22}/D_{11}] - 1)} \tag{58}$$

$$C_2 = \frac{(A - \bar{C}_{1\infty} - 3\bar{C}_{2\infty}) + [D_{22}/D_{11}](3A - 3\bar{C}_{1\infty} - \bar{C}_{2\infty})}{2([D_{22}/D_{11}] - 1)}. \tag{59}$$

In the present case the coordinates of point Q are $(0.0356, 0.0844)$.

7 Solutions with Three Interfaces

As shown by Chen [12], diffusion paths involving three moving interfaces can occur for some end member concentrations of couples composed initially of α and $\alpha + \beta$. The layer sequence and direction of each interface motion is given by $\alpha < \alpha + \beta < \alpha > \alpha + \beta$, in the notation of Morral and coworkers. Diffusion paths with intermediate layers of α phase and/or $\alpha + \beta$ phases might be expected for end member compositions for which the single interface solutions are virtual. A solution method for the three interface problem was obtained by generalizing the single interface problem using appropriate error function solutions, concentration boundary conditions from the phase diagram and flux continuity conditions.

An example of a diffusion path for a case involving three interfaces is shown in Fig. 10. The three interfaces occur at the three places where the path crosses the $\alpha/\alpha + \beta$ phase diagram boundary. The path is seen to go from the single phase region into the two phase region, returning to the single phase region before ending in the two phase region. The first two of these interfaces move towards negative x, while the third moves toward positive x. The composition jumps are consistent with Section 3.

For the same variation of end member concentration used for Fig. 6, the λ values for the three interfaces (with $\lambda_1 < \lambda_2 < 0 < \lambda_3$ representing the three interfaces in $\alpha < \alpha + \beta < \alpha > \alpha + \beta$, respectively) are given in Fig. 11. Solutions involving three moving interfaces exist only over part of the range. Also shown in Fig. 11 are the nonvirtual segments of the λ curve from Fig. 6 for the single interface solution that merge exactly with the three interface solutions. For every end member composition where the single interface diffusion path is virtual, a three interface solution exists. For every end member composition where the single interface diffusion path is nonvirtual, no three interface solution exists. On the left side of the concentration range, where three interface solutions exist, λ_1 and λ_2 converge as λ_3 merges with the single interface solution. This represents the disappearance of the intermediate $\alpha+\beta$ layer in $\alpha < \underline{\alpha+\beta} < \alpha > \alpha+\beta$ (shown underlined) to become $\alpha > \alpha+\beta$ as the value of the end member composition is changed. On the right side of the concentration range, where three interface solutions exist, λ_2 and λ_3 converge at $\lambda = 0$ as λ_1 merges with the single interface solution. This convergence represents the disappearance of the intermediate α layer in $\alpha < \alpha+\beta < \underline{\alpha} > \alpha+\beta$ (shown underlined) to become $\alpha < \alpha+\beta \mid \alpha+\beta$. The converged interface becomes the stationary interface at the origin $\xi = 0$ representing the "zigzag." Finally Fig. 12 shows the calculated microstructure map; i.e., the regions of the phase diagram where the three types of diffusion paths/microstructures are predicted to occur as the α phase end member composition is varied: 1) $\alpha > \alpha+\beta$, 2) $\alpha < \alpha+\beta|\alpha+\beta$, and 3) $\alpha < \alpha+\beta < \alpha > \alpha+\beta$.

8 Discussion and Conclusions

Diffusion through a multiphase material with an evolving microstructure presents a considerable modeling challenge. Techniques such as the computationally intense phase field method [14] have successfully described the details of solute diffusion and phase change through a two phase (mushy zone) of a solidifying binary alloy. The extension of the phase field method to ternary multiphase diffusion couples seems quite plausible. Although the present approach to ternary multiphase diffusion requires many simplifying assumptions, a wider range of problems may be treated. These assumptions, which are identical to those of Hopfe and Morral [7], are: a) local equilibrium (neglecting curvature effects) is maintained; b) the phase fraction of β is small and diffusion occurs only in the α phase matrix of the $\alpha+\beta$ mixture; c) the phase boundary is straight, and d) the diffusivities are independent of composition. In addition, we have assumed the ties lines to be parallel, The assumption that the phase fraction of β is small is valid for many applications and decreases the error associated with neglecting the diffusion in the β phase. Engström et al. [15] incorporate a labyrinth factor wherein the matrix diffusion coefficients are reduced by an empirical function of the matrix phase fraction. This is a way to include the effect of blocking of the matrix diffusion by isolated β particles. Other approaches are possible that treat the two phase mixture in an average way that depends on assumed microstructural patterns and involves the field of homogenization theory. Assumptions c) and d) become more valid as the difference in initial end member compositions becomes small. Chen and Morral [13] have determined the effects of non-parallel tie lines. In a two-phase region in the Ni-Al-Cr system, they compared error function solutions to numerical solutions using DICTRA that considered the composition-dependence of the diffusion coefficients. They found that while large differences in the effective diffusivity were calculated, the differences in the predicted diffusion paths were small.

The assumption that local equilibrium is maintained implicitly requires that no supersaturation is possible because there is no nucleation barrier to the formation of the β phase. Due to the structural heterogeneities present in solids, such an assumption is more likely to be valid in solid state diffusion couples than in those involving nucleation of a new phase from a liquid. As in the present work, Coriell et al. [16] found multiple solutions for a liquid/solid (L/S) couple in which heat and a single solute diffused. These authors performed an analysis of single phase layers and did not treat the possibility of two phase layers (mushy zones) nor did they treat the possibility of solutions with three interfaces (which would have created L/S/L/S diffusion couples. Thus they were unable to find a unique solution for all end member compositions and temperatures. In the present work, it was found that by allowing the formation of two phase layers (i.e., forbidding virtual paths) and also allowing the possibility of three interface solutions ($\alpha < \alpha + \beta < \alpha > \alpha + \beta$), the nonuniqueness problem was eliminated. Whether this happens in reality depends on the extent to which a constitutional supersaturation criteria actually describes the conditions for morphological instability leading to the formation of a two-phase structure, via a solid-state analogue of dendritic growth. Alternatively, a two-phase layer could form in the constitutionally supersaturated layer if nucleation of discrete β particles occurs easily within the α matrix. In situations where layers remain planar, other criteria must be found to select which of the multiple solutions actually occurs. Coriell et al. [17] have recently suggested a method to do this involving a stability analysis and growth kinetics.

We have obtained multiple solutions to the diffusion problem for some choices of end member composition. Our Fig. 7 showing lines of constant λ is quite similar to Fig. 9 of Maugis et al. [4]. Even though they considered only single phase layers, they also found a special point about which the lines of λ rotate. Their special point also marks the corner of the region of end member compositions where multiple solutions exist. Thus this general feature seems to be present when multiple solutions exist.

The ability to predict (calculate) microstructure maps for multiple phase diffusion couples is an important step in choosing alloy compositions for many applications; e.g., coatings, oxidation, diffusion bonding, semiconductor/metal interactions. While the analysis developed here was applied to infinite diffusion couples, the basic diffusion equations and the boundary conditions can be solved numerically to treat diffusion in finite samples, a situation required for most practical situations. We note that the proof of Section 3 regarding the nature of the jump in composition (and phase fraction of β) was derived merely using the flux continuity equations at the $\alpha/\alpha+\beta$ interface. Thus its applicability is not limited to diffusion situations with similarity solutions; e.g., couples with infinite end members.

Appendix

We show that

$$\frac{rD_{11} - rsD_{12} - D_{21} + sD_{22}}{r + s} > 0. \tag{60}$$

The slopes of the $\alpha/\alpha+\beta$ phase boundary and the tie lines in a ternary isothermal section are related as given by Hillert [18]. With our notation

$$s = \frac{g_{11} + rg_{21}}{g_{12} + rg_{22}} \tag{61}$$

where $g_{ij} = \partial^2 G_m/\partial C_i \partial C_j$ with $G_m(C_1, C_2)$ the molar free energy of the α phase. The matrix g_{ij} is symmetric and positive definite for a stable phase. Using the thermodynamic description of diffusion, the diffusion constants in the α phase can be expressed as

$$D_{11} = M_{11}g_{11} + M_{12}g_{21} \tag{62}$$

$$D_{12} = M_{11}g_{12} + M_{12}g_{22} \tag{63}$$

$$D_{21} = M_{21}g_{11} + M_{22}g_{21} \tag{64}$$

$$D_{22} = M_{21}g_{12} + M_{22}g_{22} \tag{65}$$

where M_{ij}, the diffusion mobility, is symmetric and positive definite. Substituting, the expression of interest is

$$\frac{(g_{11}g_{22} - g_{12}^2)(r^2 M_{11} - 2rM_{12} + M_{22})}{g_{11} + 2rg_{12} + r^2 g_{22}} \tag{66}$$

which contains the determinant of g_{ij} and quadratic forms for g_{ij} and M_{ij}. Thus the quantity is positive for all values of r.

References

[1] Sekerka, R. F., in Lectures on the Theory of Phase Transformations, ed. H. I. Aaronson, TMS-AIME, New York, NY, 1975, p. 117-159.

[2] Kirkaldy, J. S. and Young, D. J., Diffusion in the Condensed State, The Institute of Metals, London, 1987.

[3] Coates, D. E. and Kirkaldy, J. S., Met. Trans., 1971, 2, 3467.

[4] Maugis, P., Hopfe, W. D., Morral, J. E. and Kirkaldy, J. S., Acta mater., 1997, 45, 1941.

[5] Roper, G. W. and Whittle, D. P., Metal Science, 1981, 15, 148.

[6] Beriot, E., Master's Thesis, Diffusion in Ternary One-Phase/Two Phase Diffusion Couples, University of Connecticut, 1994.

[7] Hopfe, W. D. and Morral, J. E., Acta metall. mater., 1994, 42, 3887.

[8] Morral, J. E., Jin, C., Engström, A., Ågren, J., Scripta mater., 1996, 34, 1661.

[9] Beriot, E., Hopfe, W. D. and Morral, J. E., in Solid-Solid Phase Transformations, ed. W. C. Johnson, J. M. Howe and W. A. Soffa, TMS-AIME, New York, NY, 1994, p. 1165.

[10] Engström, A., Morral, J. E. and Ågren, J., Acta mater., 1997, 45, 1189.

[11] Meisenkothen, F., Masters Thesis, Interdiffusion Microstructure Maps for $\gamma + \gamma'/\gamma + \beta$ Ni–Cr–Al, University of Connecticut, 1998.

[12] Chen., H., University of Connecticut, unpublished research, 1999.

[13] Chen, H. and Morral, J. E., Acta mater., 1999, 47, 1175.

[14] Warren, J. A. and Boettinger, W. J., Acta metall. et mater., 1995, 43, 689.

[15] Engström, A., Hoglund, L. and Ågren, J., Met. Trans. 1994, 25A ,1127.

[16] Coriell, S. R., McFadden, G. B., Sekerka, R. F. and Boettinger, W. J., J. Crystal Growth, 1998, 191 573.

[17] Coriell, S. R., McFadden, G. B. and Sekerka, R. F., J. Crystal Growth, 1999, 200, 276.

[18] Hillert, M., Phase Equilibria, Phase Diagrams and Phase Transformations, Cambridge University Press, Cambridge, U.K., 1998, p. 277.

Figure Captions

Figure 1 Examples of diffusion paths with fixed $\alpha + \beta$ end member composition for two different α phase end member compositions. Case 1, $\lambda > 0$: the $\alpha + \beta$ two-phase mixture dissolves. Case 2, $\lambda < 0$: the $\alpha + \beta$ two-phase mixture grows. A straight line described by Eqn. (56) gives the α end member compositions where $\lambda = 0$ (i.e., a stationary interface). The line ends at the two-phase boundary at (0.06,0.06), a composition which is the end of the tie line containing the $\alpha + \beta$ end member composition (0.07, 0.07).

Figure 2 Concentration profiles for Case 1 where the $\alpha + \beta$ mixture dissolves ($\lambda > 0$, see Fig. 1). The values of $\xi = x/\sqrt{t}$ are normalized with respect to $\sqrt{D_{22}}$. The interface is located at $\xi = \lambda = 0.606\sqrt{D_{22}}$. Note the jump in the concentrations at the interface.

Figure 3 Concentration profiles for Case 2 where the $\alpha + \beta$ mixture grows ($\lambda < 0$, see Fig. 1). The values of ξ are normalized with respect to $\sqrt{D_{22}}$. The $\alpha/\alpha + \beta$ interface is located at $\xi = \lambda = -3.2\sqrt{D_{22}}$. Note that there is no jump in the concentrations at the interface. A stationary "interface" is located at $\xi = 0$ and corresponds to the location of the "zig-zag" of the diffusion path.

Figure 4 Profiles of phase fraction of β for Case 1 ($\lambda > 0$, see Fig. 1). The phase fraction is normalized by the value at $x = \infty$.

Figure 5 Profiles of phase fraction of β for Case 2 ($\lambda < 0$, see Fig. 1). The phase fraction is normalized by the value at $x = \infty$.

Figure 6 Value of λ (giving the $\alpha/\alpha+\beta$ interface speed and direction) as a function of $C_{1\infty}^{\alpha}$ for fixed values of $\overline{C}_{1\infty} = \overline{C}_{2\infty} = 0.07$ and $C_{2\infty}^{\alpha} = 0.082$. The dashed portion of the curve between the bold points represents those values of λ for which the associated diffusion paths are virtual (i.e., they involve supersaturation). The values of λ are normalized with respect to $\sqrt{D_{22}}$.

Figure 7 a) Phase diagram with superimposed straight lines indicating values of the α phase end member composition along which $\lambda/\sqrt{D_{22}}$ has the indicated values. The $\alpha + \beta$ end member composition is (0.07, 0.07). The region to the left of point P contains crossing lines that reveal the region of multiple solutions. b) enlarged view of same.

Figure 8 Phase diagram indicating regions of the α phase end member composition where multiple solutions and virtual solutions exist to the single moving interface problems, given by $\alpha > \alpha + \beta$ and $\alpha < \alpha + \beta | \alpha + \beta$, ($\lambda > 0$ and $\lambda < 0$, respectively).

Figure 9 Diffusion paths when α end member composition is located at special points P and Q.

Figure 10 Expanded view near the $\alpha < \alpha+\beta$ phase diagram boundary of the diffusion path for a three interface solution for an α phase end member composition (0.03,0.085) located in region RPQ of Fig. 8. The path consists of $\alpha < \alpha + \beta < \alpha > \alpha + \beta$. The two-phase end member composition is (0.07, 0.07).

Figure 11 Similar plot to Fig. 6 but with virtual single interface solutions eliminated and three interface solutions added. The solid vertical lines give the transition among the indicated microstructures. The dashed vertical lines indicate the multiple solution range for comparison to Fig. 6.

Figure 12 Phase diagram with superimposed regions of the α phase end member composition that produce the indicated diffusion paths (microstructure map).

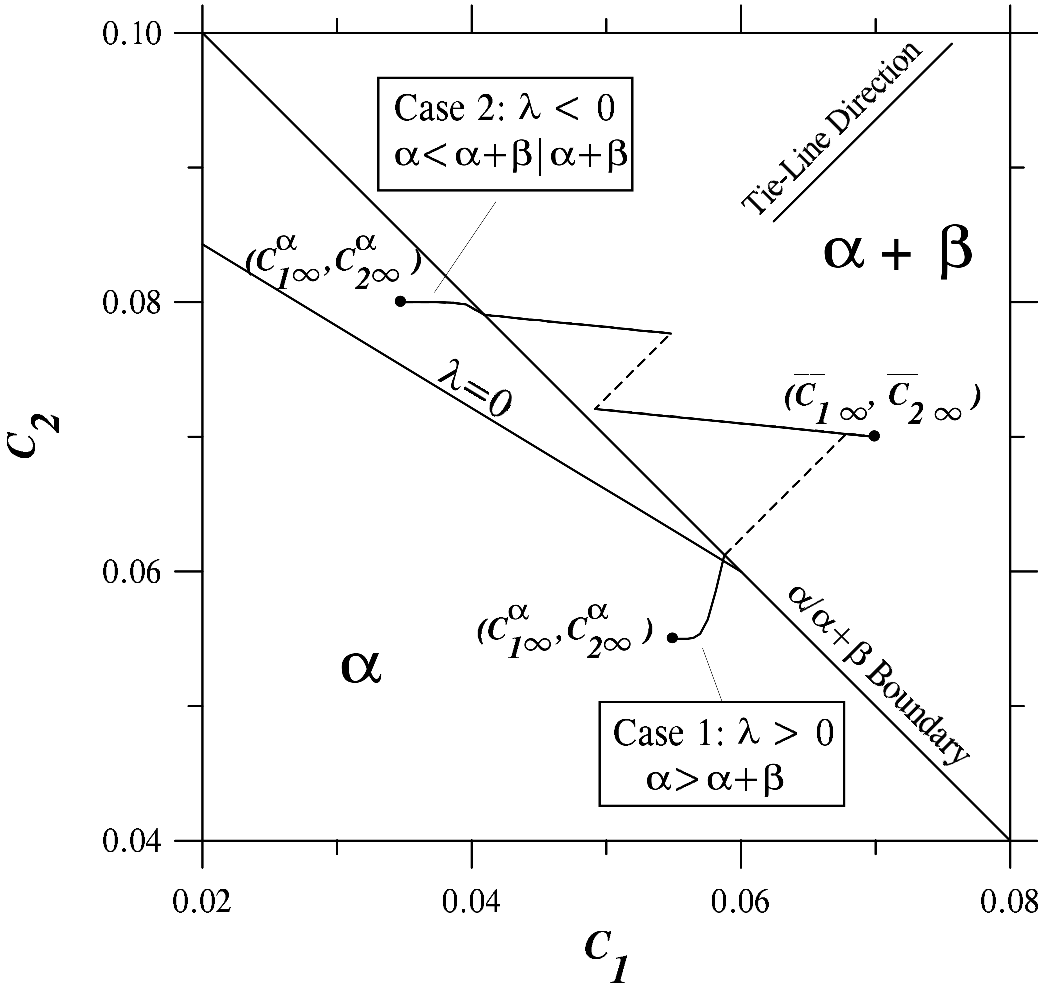

Figure 1: Examples of diffusion paths with fixed $\alpha+\beta$ end member composition for two different α phase end member compositions. Case 1, $\lambda > 0$: the $\alpha + \beta$ two-phase mixture dissolves. Case 2, $\lambda < 0$: the $\alpha + \beta$ two-phase mixture grows. A straight line described by Eqn. (56) gives the α end member compositions where $\lambda = 0$ (i.e., a stationary interface). The line ends at the two-phase boundary at (0.06,0.06), a composition which is the end of the tie line containing the $\alpha + \beta$ end member composition (0.07, 0.07).

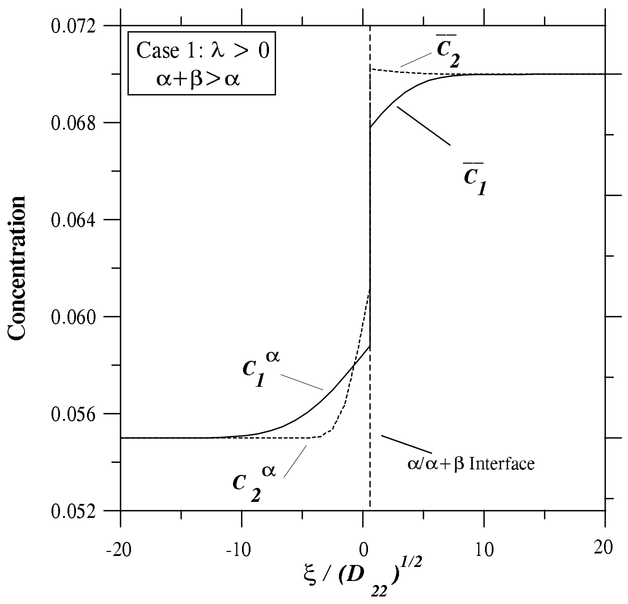

Figure 2: Concentration profiles for Case 1 where the $\alpha + \beta$ mixture dissolves ($\lambda > 0$, see Fig. 1). The values of $\xi = x/\sqrt{t}$ are normalized with respect to $\sqrt{D_{22}}$. The interface is located at $\xi = \lambda = 0.606\sqrt{D_{22}}$. Note the jump in the concentrations at the interface.

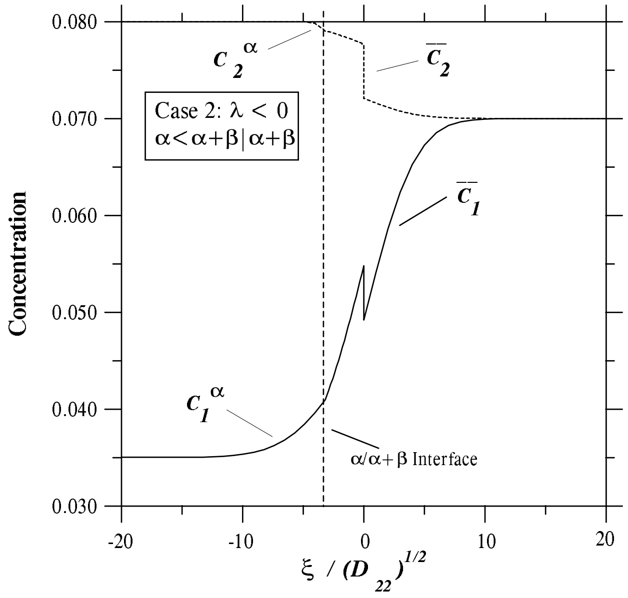

Figure 3: Concentration profiles for Case 2 where the $\alpha + \beta$ mixture grows ($\lambda < 0$, see Fig. 1). The values of ξ are normalized with respect to $\sqrt{D_{22}}$. The $\alpha/\alpha+\beta$ interface is located at $\xi = \lambda = -3.2\sqrt{D_{22}}$. Note that there is no jump in the concentrations at the interface. A stationary "interface" is located at $\xi = 0$ and corresponds to the location of the "zig-zag" of the diffusion path.

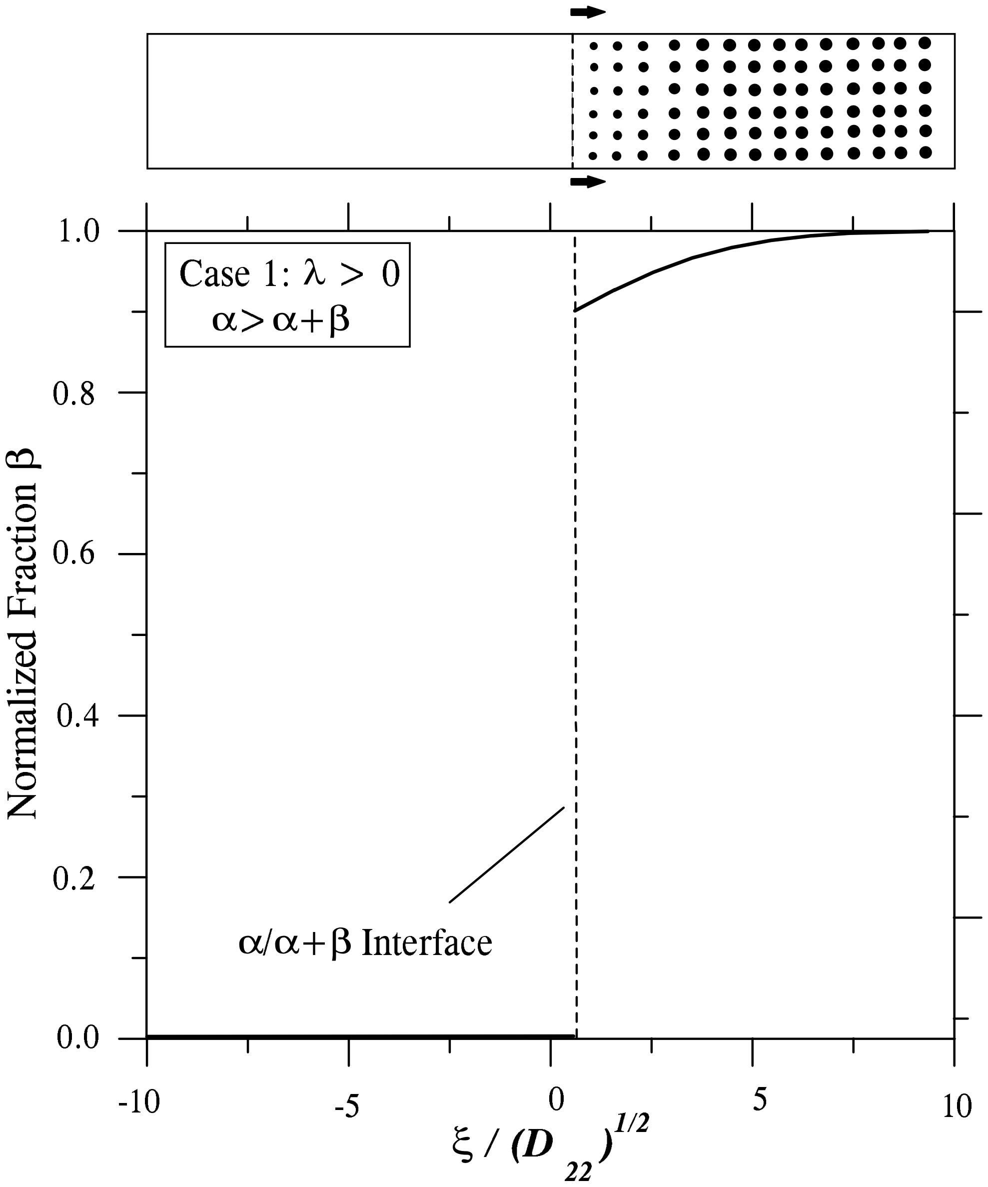

Figure 4: Profiles of phase fraction of β for Case 1 ($\lambda > 0$, see Fig. 1). The phase fraction is normalized by the value at $x = \infty$.

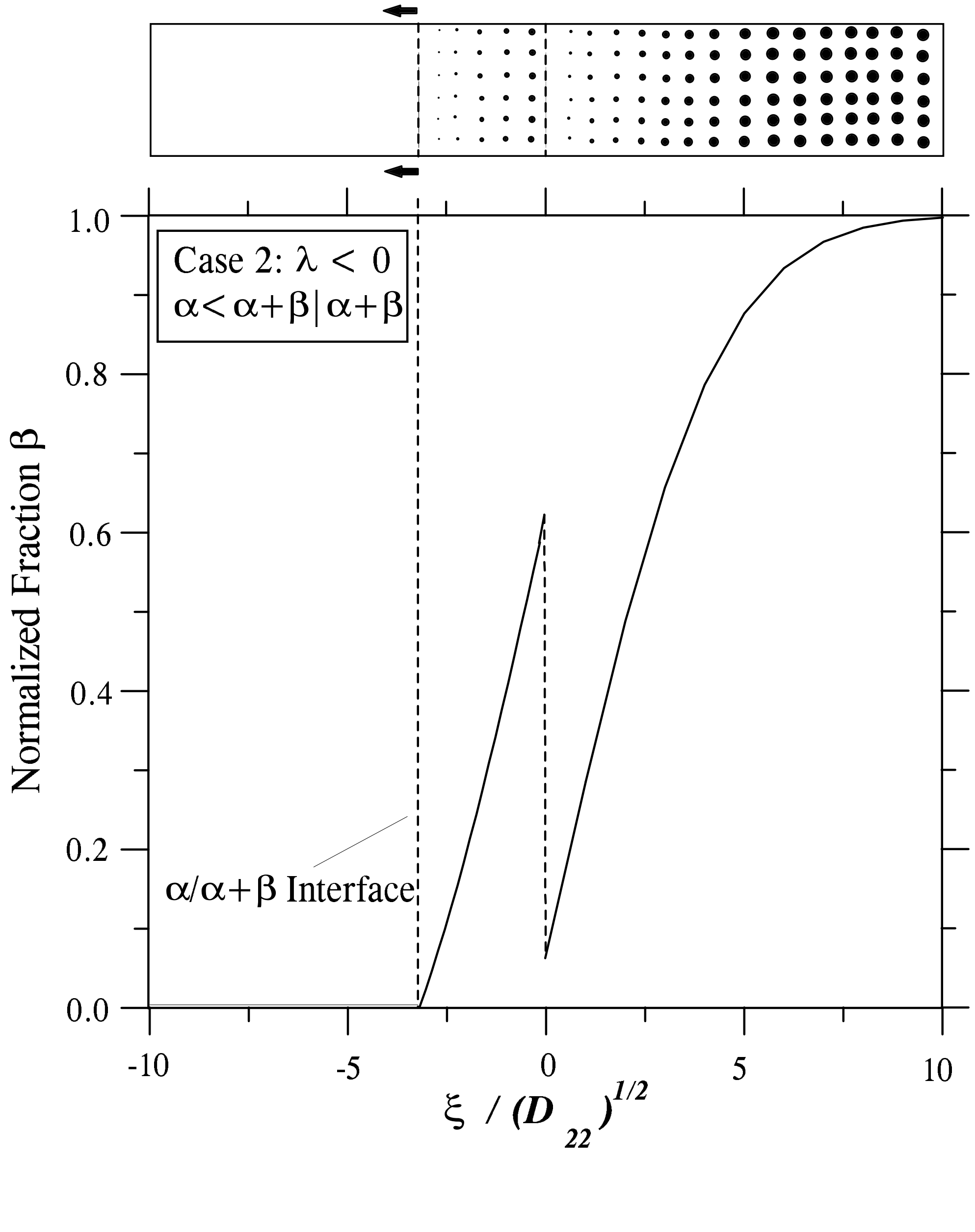

Figure 5: Profiles of phase fraction of β for Case 2 ($\lambda < 0$, see Fig. 1). The phase fraction is normalized by the value at $x = \infty$.

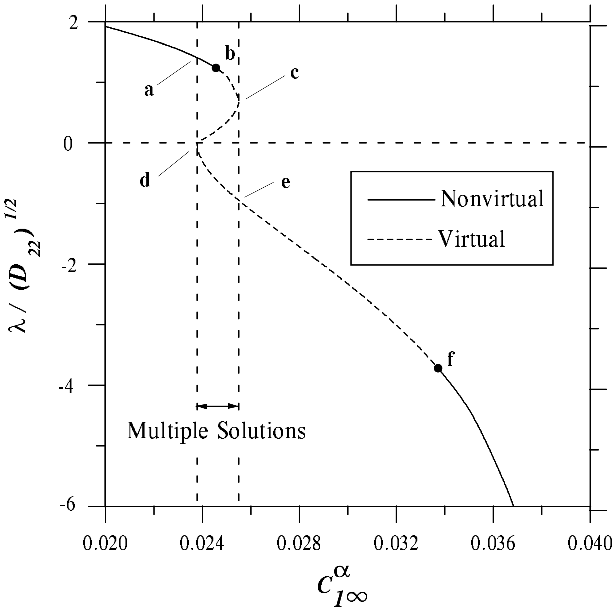

Figure 6: Value of λ (giving the $\alpha/\alpha+\beta$ interface speed and direction) as a function of $C^{\alpha}_{1\infty}$ for fixed values of $\overline{C}_{1\infty} = \overline{C}_{2\infty} = 0.07$ and $C^{\alpha}_{2\infty} = 0.082$. The dashed portion of the curve between the bold points represents those values of λ for which the associated diffusion paths are virtual (i.e., they involve supersaturation). The values of λ are normalized with respect to $\sqrt{D_{22}}$.

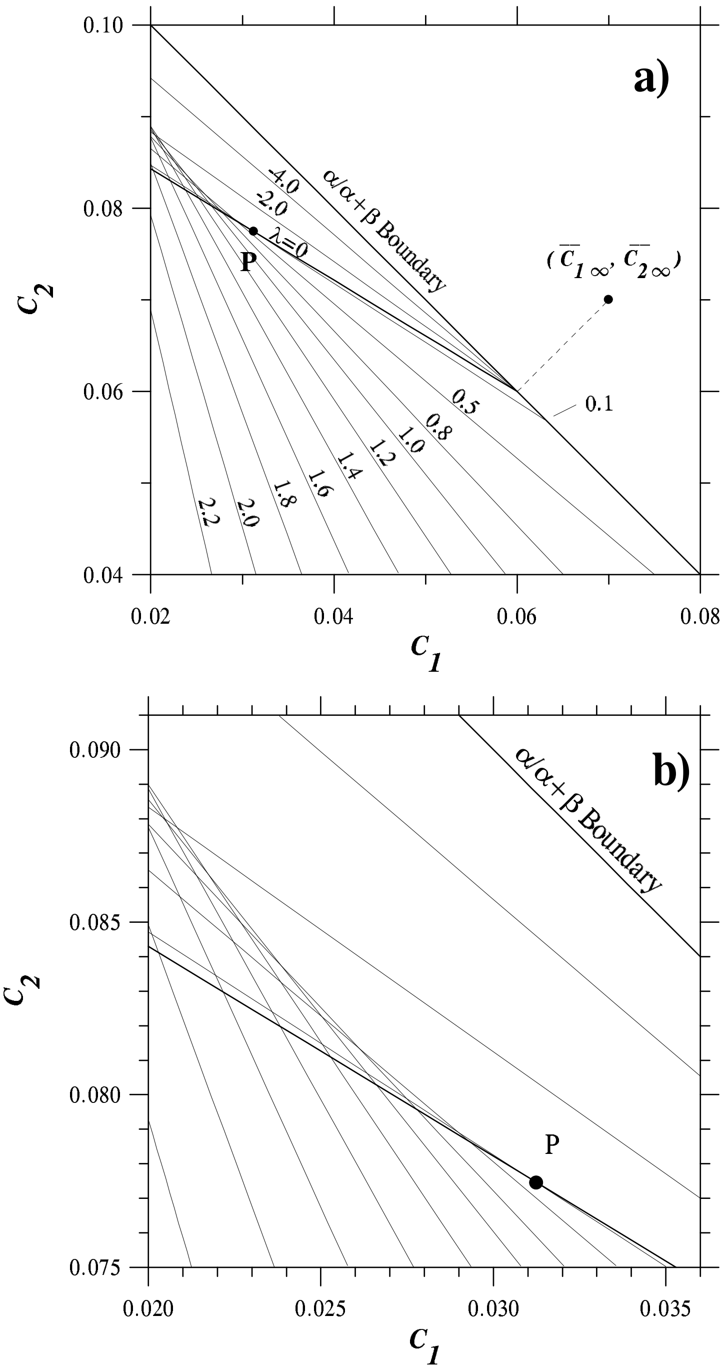

Figure 7: (a) Phase diagram with superimposed straight lines indicating values of the α phase end member composition along which $\lambda/\sqrt{D_{22}}$ has the indicated values. The $\alpha+\beta$ end member composition is (0.07, 0.07). The region to the left of point P contains crossing lines that reveal the region of multiple solutions. b) enlarged view of same.

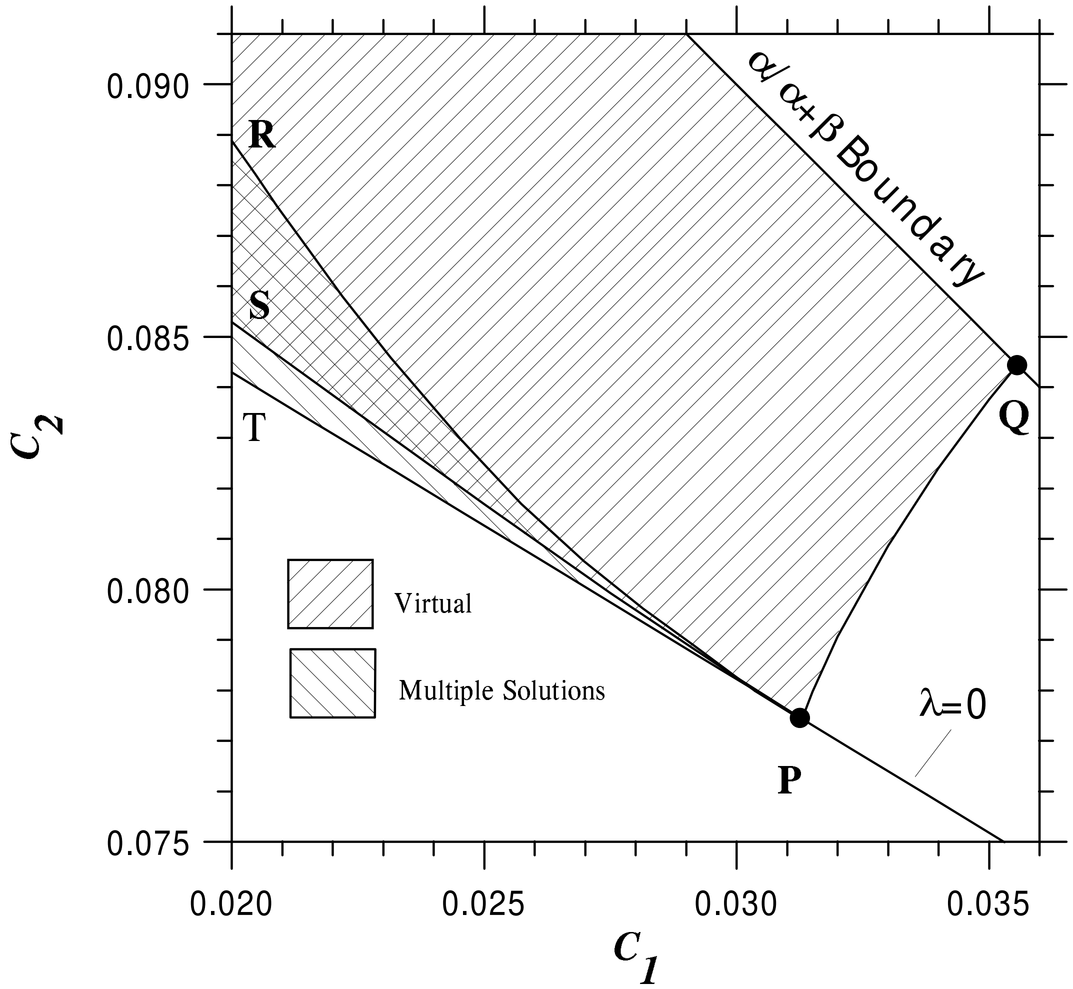

Figure 8: Phase diagram indicating regions of the α phase end member composition where multiple solutions and virtual solutions exist to the single moving interface problems, given by $\alpha > \alpha + \beta$ and $\alpha < \alpha + \beta | \alpha + \beta$, ($\lambda > 0$ and $\lambda < 0$, respectively).

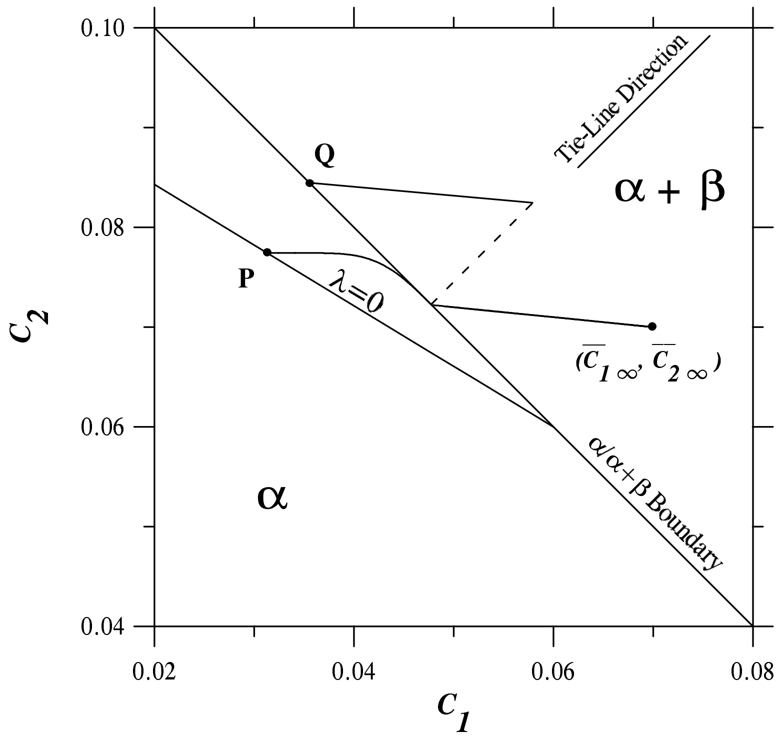

Figure 9: Diffusion paths when α end member composition is located at special points P and Q.

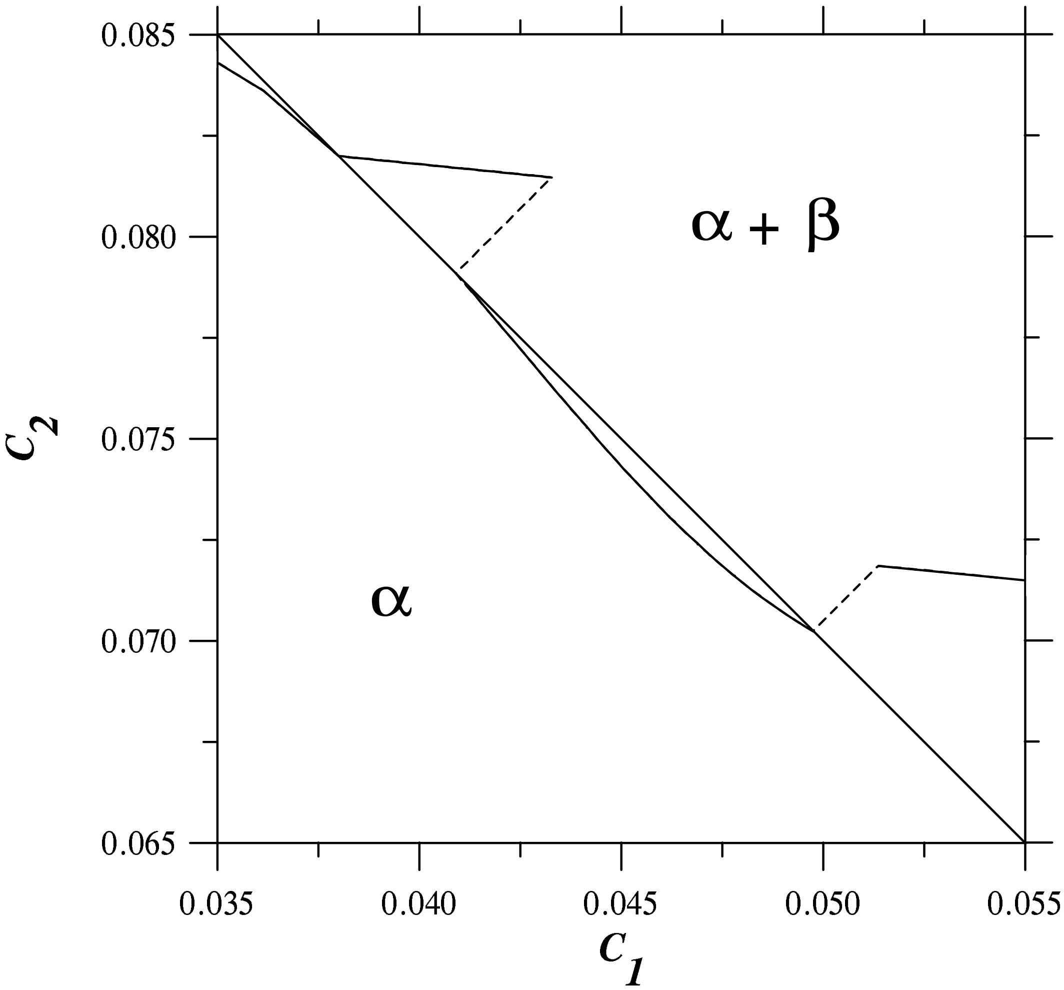

Figure 10: Expanded view near the $\alpha < \alpha + \beta$ phase diagram boundary of the diffusion path for a three interface solution for an α phase end member composition (0.03,0.085) located in region RPQ of Fig. 8. The path consists of $\alpha < \alpha + \beta < \alpha > \alpha + \beta$. The two-phase end member composition is (0.07, 0.07).

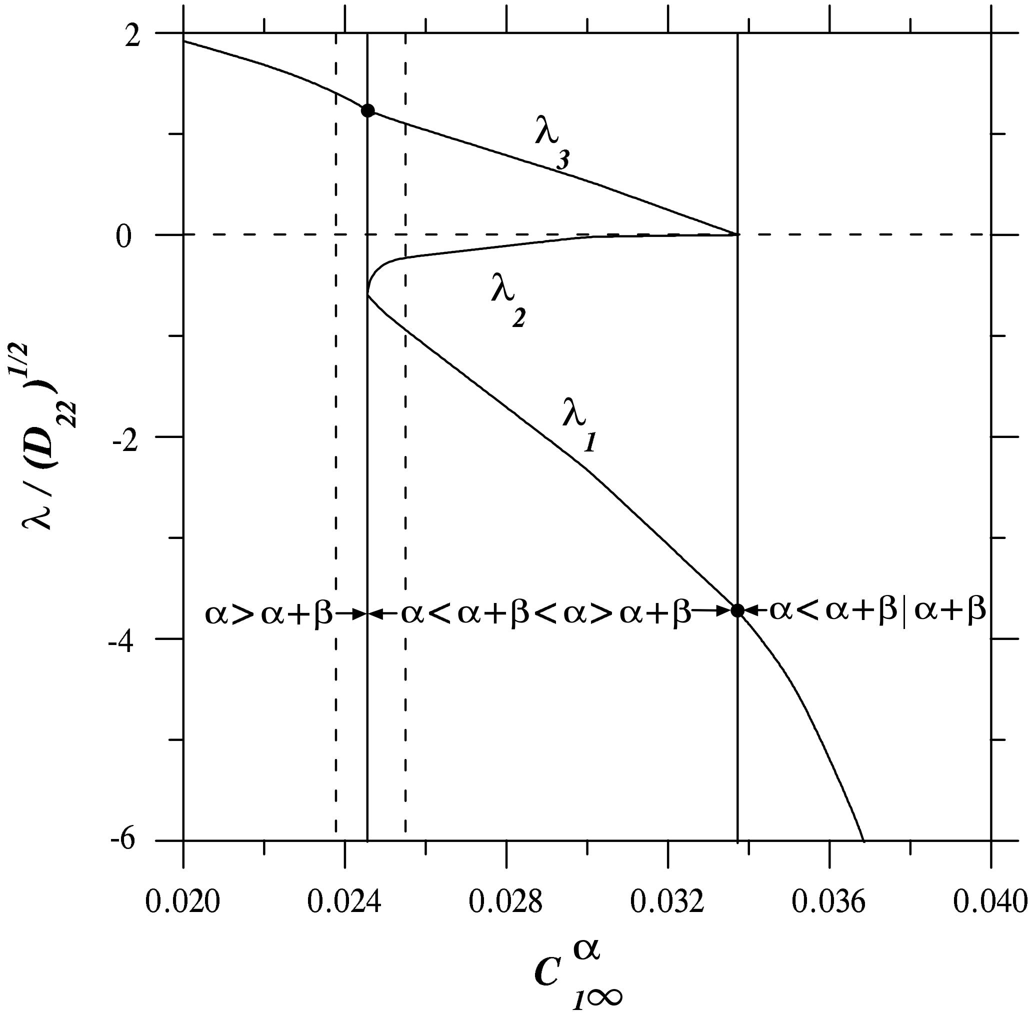

Figure 11: Similar plot to Fig. 6 but with virtual single interface solutions eliminated and three interface solutions added. The solid vertical lines give the transition among the indicated microstructures. The dashed vertical lines indicate the multiple solution range for comparison to Fig. 6.

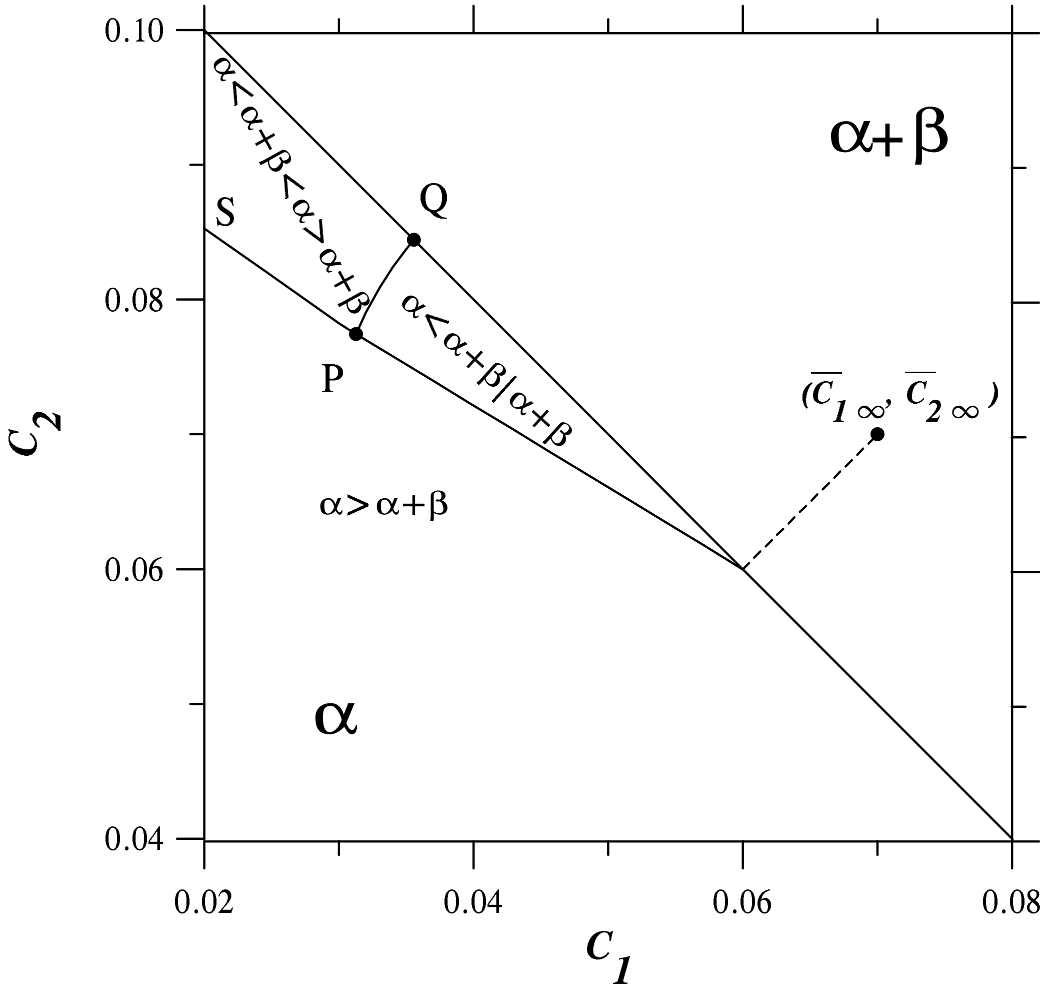

Figure 12: Phase diagram with superimposed regions of the α phase end member composition that produce the indicated diffusion paths (microstructure map).